Asian Journal of Chemistry; Vol. 37, No. 6 (2025), 1477-1486

ASIAN JOURNAL OF CHEMISTRY

https://doi.org/10.14233/ajchem.2025.33849

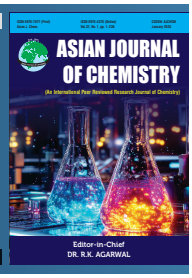

Impact of Graphene Oxide and Zinc Oxide Nanofillers on Polyvinyl Alcohol Polymer Matrix

SANOOP PADINHATTAYIL[1,*], K. SHESHAPPA RAI[1] and BIBIN SHAJI[2]

[1]Department of Post-Graduate Studies and Research in Polymer Science, University of Mysore, Sir M. Visvesvaraya Post-Graduate Centre, Tubinakere, Mandya-571402, India
[2]Department of Post-Graduate Studies and Research in Chemistry, University of Mysore, Sir M. Visvesvaraya Post-Graduate Centre, Tubinakere, Mandya-571402, India

*Corresponding author: E-mail: sanoop.home@gmail.com

Received: 11 April 2025; *Accepted*: 20 May 2025; *Published online*: 27 May 2025; AJC-22021

This study offers a comparative analysis and analogy of polymer nanocomposites that utilize the well-established polymer matrix polyvinyl alcohol (PVA), enhanced with graphene oxide (GO) and zinc oxide (ZnO) nanoparticles as nano-fillers. The polymer nanocomposite films were fabricated using a solution casting technique and were subsequently characterized through infrared spectroscopy, X-ray diffraction (XRD) analysis, assessments of mechanical properties, thermal characterization and optical microscopy. The addition of GO and ZnO nanoparticles led to significant changes in the structural, thermal, mechanical and optical properties of the PVA polymer. Specifically, the thermal stability of the composite films showed improvement compared to pure PVA, although the mechanical analysis revealed a significant increase in tensile strength.

Keywords: Polyvinyl alcohol, Graphene oxide, Nanocomposites, Mechanical property, Electrical property.

INTRODUCTION

Organometallic polymers, characterized by their low basic weight and remarkable chemical resistance, have attracted considerable attention from academic researchers across various disciplines, including chemistry and solid-state physics [1]. A key advantage of these materials is the ability to customize their properties, leading to enhancements in strength and processability compared to the original polymer. Observing changes in the polymer structure is essential in some instances to adjust the physical properties necessary for specific applications. Incorporating suitable metal ions into the polymer chain makes it feasible to alter the polymer composition and introduce new performance characteristics [1]. Additionally, graphene composites, particularly graphene oxide (GO), have emerged as a valuable resource due to their widespread applications in areas such as sensors, energy sources, fuel cells and nanocomposites [2-5]. Nanocomposites that incorporate graphene oxide with polymers are more intriguing than standard polymers due to their unique properties [6,7]. Polyvinyl alcohol, a synthetic polar polymer, serves as an outstanding host material due to its impressive thermal stability, resistance to chemicals, ability to form films, non-toxic nature, biocompatibility, biodegradability and diverse molecular weight options [8]. The uniform dispersion of graphene oxide (GO) within polyvinyl alcohol (PVA) enhances various physical and mechanical characteristics, along with thermal stability and electrical conductivity, at the molecular level [9-12]. Composites based on PVA/GO were being manufactured for various applications [13,14].

ZnO is a thoroughly researched n-type semiconductor material, characterized by a specific band gap that ranges from 3.2 to 3.4 eV at room temperature. It is part of the II-VI semiconductor family and possesses distinctive physical properties, including a low growth temperature, compatibility with a wide range of natural substrates, excellent radiation resistance and a high exciton binding energy of 60 meV [15,16]. These findings indicated that ZnO can form unique nanostructures such as nano rings, nano wires, nano rods, nano springs, nano helices and nano clusters due to the polar characteristics of its surface is noteworthy, as these structures are rarely observed in other oxides [17]. ZnO is well-suited for a variety of electronic and optoelectronic applications, including varistors [18], high power transparent electronics, chemical sensors, biosensors [19], gas sensors, transparent conducting electrodes, dye sensitized solar

cells [20], solar panels, ultraviolet laser diodes, photovoltaics and engineered modules for telecommunications. Numerous efforts have been made to enhance the optical, mechanical and thermal properties of ZnO nanostructures and the integration of ZnO nanoparticles with PVA has been shown to improve their electrical, biological, mechanical and optical characteristics.

EXPERIMENTAL

All chemicals utilized in this research were of analytical quality. Polyvinyl alcohol (PVA) was sourced from Merck India Ltd., India with a molecular weight of 125,000 Daltons. Graphite flakes, sized at 60 meshes, were acquired from Loba Chemie. Zinc sulfate, zinc acetate dihydrate, sodium hydroxide, sulfuric acid, hydrochloric acid, ethanol, hydrogen peroxide, potassium permanganate and sodium nitrate were obtained from S.D. Fine Chemicals, India. Double-distilled water was employed in the preparation of the composite films.

Preparation of PVA/ZnO and PVA/GO nanocomposites: ZnO nanoparticles were synthesized through a precise precipitation technique [21]. A molar ratio of 1:2 was gradually added to an aqueous solution containing zinc sulfate and NaOH while being vigorously stirred for approximately 12 h. The resulting precipitate was then filtered, rinsed with deionized water and dried in a hot air oven at 100 ºC. The collected powder underwent calcination in a muffle furnace for 2 h at 550 ºC. The resulting ZnO nanoparticles were characterized using XRD and FTIR and the average particle size was obtained as 26.74 nm.

Graphene oxide (GO) was synthesized using a modified Hummer's method [22] and the average crystal size of the GO nanomaterials was determined to be 35.20 nm through the application of Scherrer's formula [21].

Solution casting is an effective and versatile method for producing nanocomposite films on a laboratory scale. In the preparation of polymer nanocomposites, 4 g of PVA are dissolved in 100 mL double double-distilled water at 70-80 ºC and combined with GO nanoparticles and ZnO nanoparticles in the same medium separately. This mixture was subjected to sonication for 30 min, followed by continuous stirring for 1 h. The resulting homogeneous solution was then poured onto a glass plate. The solvent was eliminated *via* evaporation, after which the dried film was meticulously detached from the substrate and preserved in a desiccator for further investigation.

Characterization: The X-ray diffractometer (XRD) analysis for the PVA and the composite structure of PVA/GO-ZnO nanocomposite was conducted using a Bruker diffractometer (model 8600, USA) employing Cu*K*α radiation (k = 0.15406 nm). The instrument was operated at a voltage of 40 kV, with a scanning rate of 2º/min across a range of 10º to 80º (2θ) angles. FTIR spectra for pure PVA and the various nanocomposite films were recorded with Perkin-Elmer ABB FTIR spectrophotometer over a range of 4000 to 550 cm^{-1}. The thermal characteristics of the PVA/GO and PVA/ZnO nanocomposite films were analyzed using a Perkin-Elmer DSC/TGA instrument (model Exstar, Japan). The nanocomposite films were heated at a rate of 30 ºC/min in a nitrogen atmosphere. Optical analysis was conducted using a UV-1800 spectrophotometer from Shimadzu, Japan. The Tauc equation was employed to determine the band gap energy (E_g) of the PVA and PVA/GO-ZnO nanocomposite films.

A key characteristic of numerous materials is sheet resistance, also referred to as surface resistivity, which measures the capacity of charge carriers to traverse uniform thin films. The four-probe technique is the most suitable method for assessing sheet resistance. This technique employs four equally spaced, collinear probes, known as a four-point probe, to establish electrical contact with the material. Typically, commercially available four-point probes feature sharp needle-like tips. The four-probe method operates by inserting four collinear probes into the material, with the outer probes (1 and 4) applying a direct current (DC), while the voltage drop is measured between the inner probes (2 and 3). Subsequently, the sheet resistance can be calculated using the following equation:

$$\rho = 2\pi s\left(\frac{V}{I}\right)$$

In this context, V represents the voltage difference in volts measured between the internal probes; I denotes the current flowing through the outer pair of ampere probes; and S denotes the distance between the meter probes.

RESULTS AND DISCUSSION

XRD spectral studies: The XRD technique plays a crucial role in evaluating the arrangement and distribution of graphene oxide (GO) within the polyvinyl alcohol (PVA) polymer matrix. Fig. 1 illustrates the representative XRD patterns for both PVA and PVA/GO nanocomposites. The diffraction peak corresponding to GO sheets is observed at 2θ = 13.9º, which aligns with a *d*-spacing of 0.83 nm, as determined by the Bragg diffraction equation [23]. In the XRD patterns of PVA/GO composites with varying GO concentrations, no distinct GO peak is detected; instead, only the (101) diffraction peak of PVA crystal appears at 2θ = 19.7º. This phenomenon can be explained by the complete intercalation of GO sheets, which prevents restacking and allows for their uniform dispersion within the PVA matrix. Compared to the pure PVA matrix, the diffraction peaks of the nanocomposite films become broader and less intense as the nanoparticle concentration increases. This shift may be attributed to a decrease in intermolecular hydrogen bonding interactions between PVA chains, resulting from the interactions at the interface between PVA and GO [24]. As depicted in Fig. 1, the incorporation of GO nanoparticles into the PVA matrix leads to the complete absence of GO peak and the emergence of a new, singular, enhanced peak. These results indicate a uniform dispersion and effective integration of the GO nanofiller within the PVA matrix.

Fig. 2 illustrates the X-ray diffraction (XRD) patterns of polyvinyl alcohol (PVA) and PVA/ZnO nanocomposites at various weight percentages of ZnO. PVA may exhibit crystalline characteristics. The peak observed is likely attributed to the interaction between PVA and ZnO nanoparticles at specific interplanar spacings. The uniform distribution of nanoparticles enhances the high surface area of the nanocomposites, leading to an increase in the crystallinity of the polymer nanocompo-

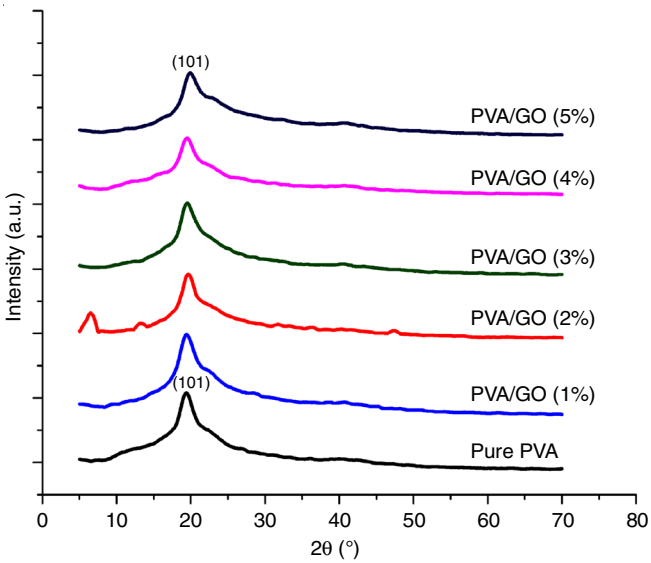

Fig. 1. XRD analysis of PVA pure and PVA/GO nanocomposites

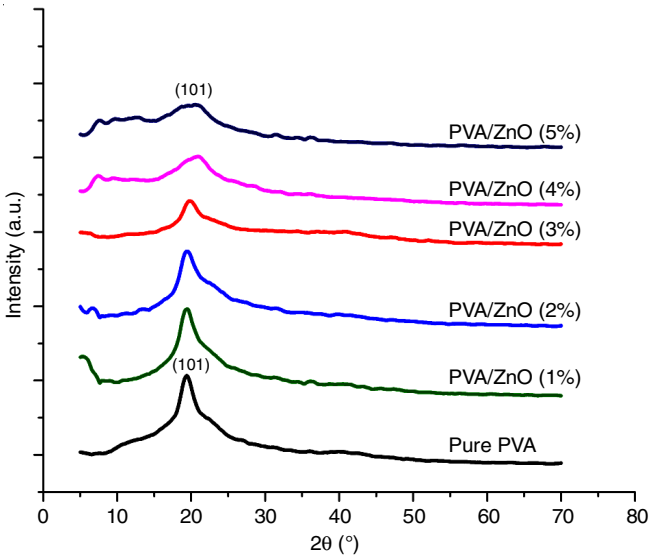

Fig. 2. XRD analysis of PVA/ZnO nanocomposites

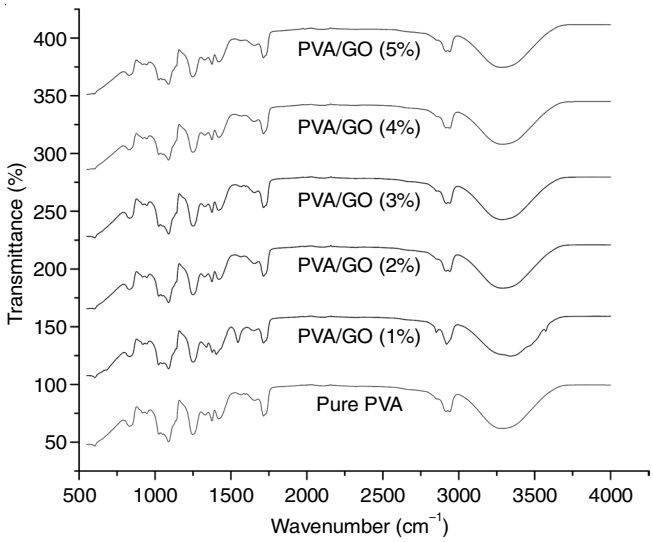

Fig. 3. FTIR spectra of pure PVA and PVA/GO nanocomposites

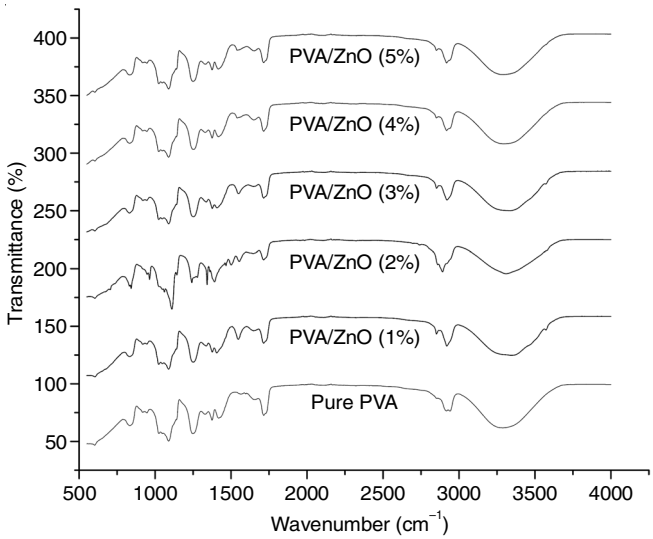

Fig. 4. FTIR spectra of pure PVA and PVA/ZnO nanocomposites

sites [25]. Consequently, the crystallinity of PVA is elevated and the diffraction peaks become more pronounced, distinguishing them from the peaks of ZnO. A comparison of the XRD patterns of the PVA/ZnO nanocomposite with those of ZnO nanoparticles reveals corresponding angles of 2θ = 36.83º, 38.45º, 41.45º and 52.70º, confirming the presence of zinc oxide within polyvinyl alcohol. The XRD patterns for pure polyvinyl alcohol, zinc oxide and their composites indicate that ZnO maintains its structural integrity even after being encapsulated with PVA during the composite formation process.

FTIR spectral studies: In absorbance mode, the FTIR spectra for pure PVA, PVA/GO and PVA/ZnO nanocomposites are illustrated in Figs. 3 and 4. The pure PVA exhibits peaks at 3300, 2938, 2850, 1721 and 1028 cm^{-1}, which correspond to O–H stretching vibrations, C–H symmetric stretching vibrations, C–H asymmetric stretching vibrations, C=O stretching vibrations and C–O stretching vibrations, respectively. FTIR analysis was conducted to gain insights into the hydrogen bonding interactions between GO and PVA. The –OH stretching bands are shown to be sensitive to hydrogen bonding. The FTIR spectra of the PVA/GO nanocomposites closely resemble those of pure PVA, as depicted in Fig. 3, indicating that the incorporation of GO influences the composition of PVA. Moreover, the –OH stretching peak shifts from 3300 cm^{-1} in pure PVA to lower wavenumbers of 3288 cm^{-1} in PVA-1% GO and 3272 cm^{-1} in PVA-5% GO, suggesting a reduction in hydrogen bonding among the hydroxyl groups within the PVA chains [26].

The peak around 3300 cm^{-1} in the spectra of pure PVA and all composites is attributed to the –OH group in the polymer backbone, while the peaks at 2917 cm^{-1} and 2854 cm^{-1} correspond to CH_2 asymmetric and symmetric stretching, respectively. The peak observed at 1413 cm^{-1} is due to C–C stretching. Moreover, the peak at approximately 658 cm^{-1} in the PVA/ZnO composites is associated with Zn–O stretching, which is absent in the neat polymer film, indicating that ZnO is integrated into the polymer matrix.

Thermal studies: The results of the thermogravimetric analysis (TGA) for pure PVA and PVA/GO films with GO loa-

TABLE-1
PERCENTAGE OF WEIGHT LOSS OF PVA/GO NANOCOMPOSITES AT DIFFERENT TEMPERATURES

Sample code	Percentage of weight loss at various temperatures						
	100 ºC	200 ºC	300 ºC	400 ºC	500 ºC	600 ºC	Residue
Pure PVA	7.3699	13.9240	25.4520	77.0180	93.5210	94.1010	2.626
PVA/GO (1%)	6.4910	11.5730	23.806	72.187	88.302	88.935	3.885
PVA/GO (2%)	3.857	8.453	20.441	75.721	92.862	93.719	1.651
PVA/GO (3%)	5.054	10.752	22.722	76.869	93.930	94.510	1.730
PVA/GO (4%)	3.030	8.428	18.080	73.443	93.402	94.225	1.003
PVA/GO (5%)	4.334	10.15	20.250	74.477	93.651	94.192	2.179

dings ranging from 1% to 5 wt.% % are presented in Fig. 5. The decomposition behaviour of all PVA films is consistent. Table-1 shows the initial weight loss approximately 10%, occurs at temperatures below 200 ºC, which is attributed to the release of adsorbed water and the breakdown of unstable oxygen functional groups within the material. The significant weight loss, ranging from 50% to 70%, takes place between 200 and 450 ºC, primarily due to the thermal degradation of the PVA matrix. Furthermore, in contrast to pure PVA, the TGA curves for the PVA and PVA/GO films shift to higher temperatures. The onset temperatures for rapid decomposition of pure PVA and PVA/GO films are approximately 230 and 280 ºC, respectively, as illustrated in Fig. 5. This indicates that the presence of GO significantly enhances the thermal stability of the PVA films.

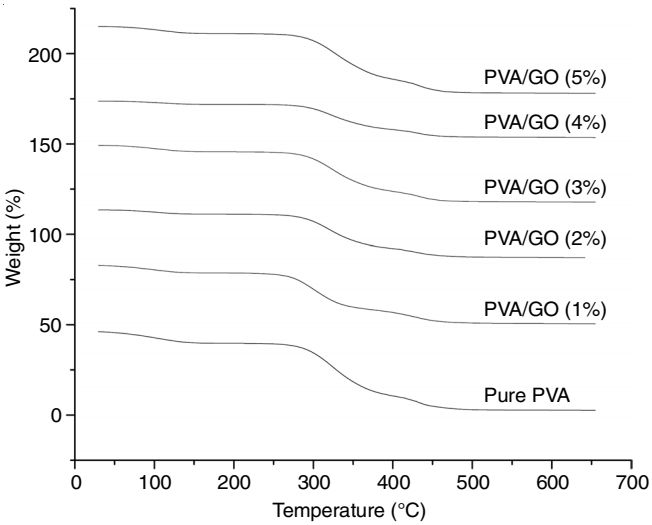

Fig. 5. TGA analysis spectra of pure PVA and PVA/GO nanocomposites

The impact of ZnO on the thermal degradation behaviour of PVA was examined through TGA, with the thermal curves for both unfilled PVA and the PVA/ZnO nanocomposite (Fig. 6). The thermal degradation of PVA reveals three distinct weight loss regions. The initial region, observed between 80 and 180 ºC, is attributed to the evaporation of weakly bound and chemically heavy water [27], where the maximum decomposition temperature reaches 158 ºC, resulting in a weight loss of approximately 6%. The second region, occurring between 250 and 420 ºC, is linked to the degradation of the PVA side-chain [28]. In this phase, the total weight loss is around 76%, with peak decomposition temperatures of 268 and 362 ºC [29]. The final stage, occurring from 420 to 490 ºC, is due to the cleavage of the C–C backbone of PVA, with a maximum decomposition temperature of 451 ºC [25]. At 800 ºC, the unfilled PVA experiences a weight loss of 96%. In contrast, the thermal degradation of PVA/ZnO also exhibits three weight loss regions, but its curves significantly differ from those of unfilled PVA. From Table-2, the first region for PVA/ZnO occurs between 80 and 230 ºC, with a maximum decomposition temperature of 211 ºC and a weight loss of about 9%. This weight loss can be attrib-

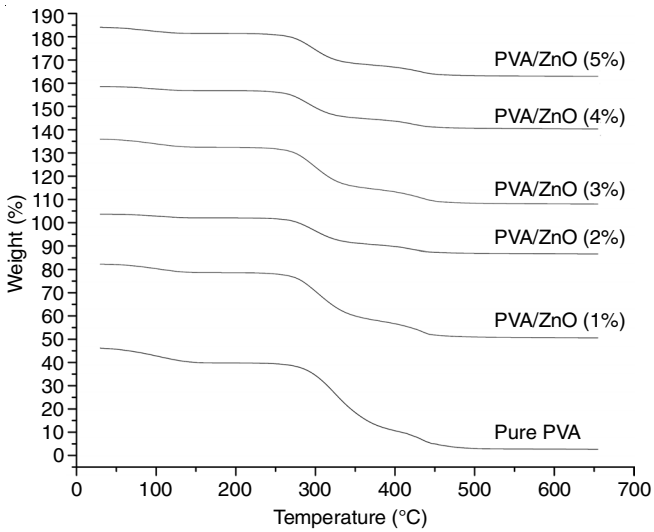

Fig. 6. TGA analysis spectra of pure PVA and PVA/ZnO nanocomposites

TABLE-2
PERCENTAGE OF WEIGHT LOSS OF PVA/ZnO NANOCOMPOSITES AT DIFFERENT TEMPERATURES

Sample code	Percentage of weight loss at various temperatures						
	100 ºC	200 ºC	300 ºC	400 ºC	500 ºC	600 ºC	Residue
Pure PVA	7.3699	13.924	25.452	77.018	93.521	94.101	2.626
PVA/ZnO (1%)	5.512	10.485	36.152	73.125	88.674	89.463	3.621
PVA/ZnO (2%)	3.656	8.433	34.389	72.090	87.286	88.370	2.013
PVA/ZnO (3%)	6.373	11.224	40.084	72.458	87.743	88.619	3.482
PVA/ZnO (4%)	4.563	8.506	40.495	70.297	85.208	86.360	2.66
PVA/ZnO (5%)	7.225	11.267	43.058	71.865	86.382	87.273	2.99

uted not only to the evaporation of unreacted materials and unsegregated byproducts but also to the loss of chemically bound and mechanically weakly bound water. Consequently, the PVA/ZnO demonstrates a higher decomposition temperature and weight loss in this region compared to unfilled PVA. The second region for PVA/ZnO, resulting from the weakening of the PVA side-chain, occurs around 300 to 400 ºC. In this phase, the total weight loss is approximately 65 wt.%, with the peak decomposition temperature reaching 356 ºC. This suggests that the incorporation of ZnO nanoparticles significantly enhances the thermal stability of PVA. This observation has been corroborated by various researchers [30-32]. The improved thermal stability can be attributed to the higher crystallinity of PVA and the restricted mobility of polymer segments due to the formation of networks comprising polymer chains and inorganic components [33]. In the third stage, the cleavage of the C–C backbone in the PVA/ZnO nanocomposite occurs between 410 and 490 ºC, which is earlier than that of the unfilled PVA. This indicates that the thermal stability of PVA in the PVA/ZnO composite is reduced compared to the unfilled PVA, following the degradation of the polymer network due to the presence of ZnO particles. The maximum decomposition temperature in this region is 445 ºC, which is lower than that of unfilled PVA. When the temperature exceeds 800 ºC, the PVA/ZnO composite experiences a weight loss of 95%.

The DSC spectra for both pure PVA and PVA/GO composites, varying in weight percentage of GO, are illustrated in Fig. 7. This figure highlights the glass transition characteristics of PVA and PVA/GO. It is observed that the glass transition temperature (T_g) of bulk PVA is approximately 74 ºC, while the T_g for PVA/GO composites containing 5% GO is around 68 ºC. This difference can be attributed to the hydrogen bonding interactions between the oxygen-containing functional groups on the GO layers and the polymer matrix. As reported [34], the crumpled morphology of the GO fillers may hinder the segmental mobility of the polymer chains. The data suggest that the incorporation of GO into PVA enhances the crystalline characteristics of the polymer while simultaneously reducing the T_g. The PVA chains are uniformly intercalated within the GO layers in the PVA/GO nanocomposites. Fig. 8 presents the DSC curves for neat PVA and PVA/ZnO nanocomposites with varying ZnO loadings. The melting temperature (T_m) of pristine PVA is recorded at 189 ºC, which gradually decreases with increasing ZnO content, reaching a minimum of 185 ºC at the highest ZnO loading of 5 wt.%. It is commonly concluded that the dispersed ZnO particles impede the folding of PVA chains and the growth of crystallinity [35]. The strong hydrogen bonding interactions between ZnO and PVA chains disrupt the orderly arrangement of the PVA chains, leading to a reduction in crystallinity and a corresponding decrease in T_m. A significant reduction in T_g from 74 to 69 ºC was also observed with an increase in nanoparticle content from 1 to 5 wt.%. This decrease in T_g indicates that the hydrogen bonds among PVA chains are weakening due to the novel interactions occurring within the nanocomposites.

Mechanical properties: The mechanical characteristics of composites are affected by their uniformity and the strong

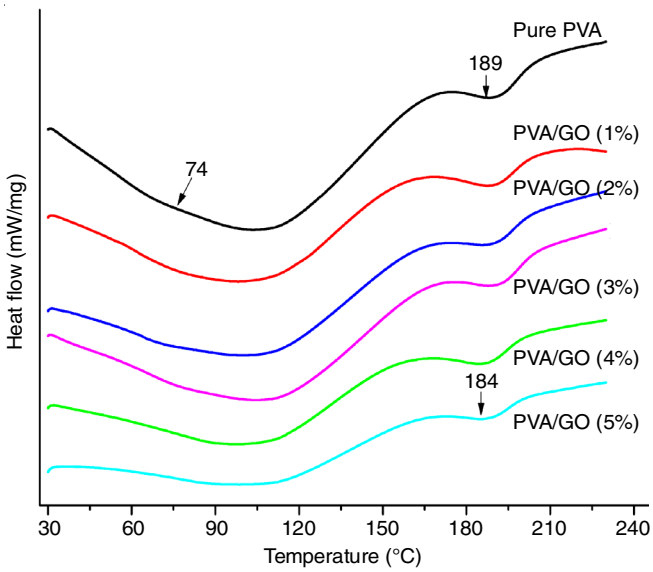

Fig. 7. DSC analysis spectra of PVA/GO nanocomposites

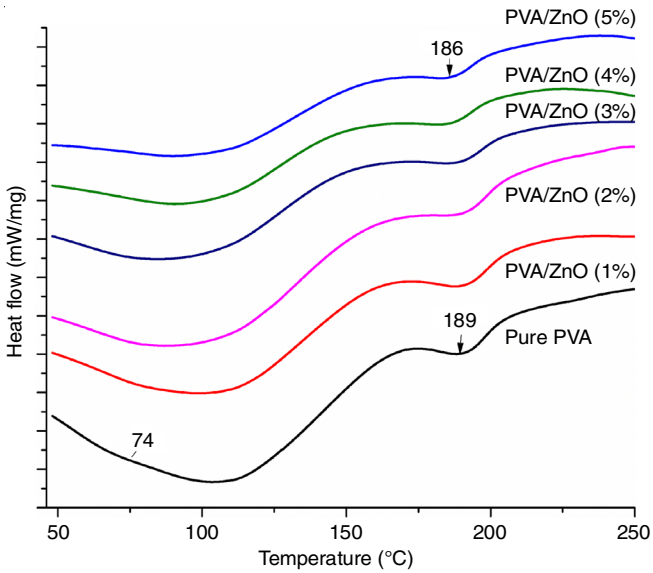

Fig. 8. DSC analysis spectra of PVA/ZnO nanocomposites

interfacial interactions between nanoparticles and the polymer matrix. Table-3 provides a detailed overview of these mechanical properties. It is evident that at lower loading speeds, both tensile strength and Young's modulus increase with the addition of graphene oxide (GO) material. Specifically, the tensile strength of PVA with 4% GO rises from 3.859 MPa to 9.613 MPa, while Young's modulus increases from 104.40 MPa to 198.80 MPa. The remarkable tensile strength (130 GPa) and Young's modulus (0.25 TPa) of GO nanoparticles [35-37], along with the excellent order and uniform distribution of GO within the polymer matrix, contribute significantly to the enhancement of mechanical properties even at low GO loading. This improvement can be attributed to strong hydrogen bonding interactions between the GO and polymer chains, as well as the aligned arrangement of GO parallel to the surface of the sample films. Moreover, the crumpled texture of the GO may develop new connections that further enhance mechanical properties. However, the slight reduction in tensile strength and Young's modulus

TABLE-3
MECHANICAL PROPERTIES OF PURE PVA AND PVA/GO, PVA/ZnO NANOCOMPOSITES

Sample name	Young's modulus (MPa)	Elongation at break (%)	Tensile strength (MPa)
Pure PVA	104.40	7.97	3.859
PVA/GO (1%)	196.256	119.7	8.294
PVA/GO (2%)	199.167	119.94	7.225
PVA/GO (3%)	198.804	119.95	9.613
PVA/GO (4%)	225.627	119.95	7.293
PVA/GO (5%)	201.50	119.83	6.101
PVA/ZnO (1%)	142.052	9.93	2.866
PVA/ZnO (2%)	157.342	19.92	5.695
PVA/ZnO (3%)	129.591	119.68	9.307
PVA/ZnO (4%)	181.273	119.78	8.04
PVA/ZnO (5%)	179.434	119.97	8.816

observed in PVA with 4% and 5% GO content can be attributed to incomplete intercalation, which diminishes the effectiveness of the mechanical enhancement.

Pure PVA exhibits the lowest tensile strength and Young's modulus, while it demonstrates the highest percentage of strain at its weakest point (Table-3). As anticipated, both tensile strength and Young's modulus increased across all treatments with varying concentrations of ZnO. An increase in ZnO nanoparticle concentration to 3% resulted in observed enhancements in the tensile strength and Young's modulus; however, a further increase to 5% led to a decline in these properties. This reduction may be attributed to the aggregation of nanoparticles. Consequently, the mechanical properties can be modified through the incorporation of ZnO nanoparticles, provided that the concentration allows for an even distribution of the nanomaterials within the PVA, maintaining a uniform structure [38].

Optical studies: The absence of an absorption peak in the visible region for pure PVA suggests that the film is transparent (Fig. 9), whereas the nanocomposite films exhibit an absorption peak at 416 nm, likely due to an electronic transition involving the *d*-orbitals of the nanoparticles. The absorbance spectra of PVA/GO with varying weight percentages of GO (1-5%) are presented within the 200-800 nm wavelength range. The observed absorption peak between 260-380 nm corresponds to the transformation of the C=C bond in GO (Fig. 10), attributed to the surface plasmon resonance, which occurs when electrons transition from a specific energy level [39]. By extrapolating the steep portion of the absorption curve to intersect the photon energy axis, the optical band gap values were determined. The transmittance edge was calculated for different weight percent formulations, revealing a consistent reduction in the transmission edge. These defects contribute to localized states within the optical band gap [40-42] resulting in the alterations to the optical band energy. The optical band energy was assessed using the Tauc plot, with the various compositions of PVA/GO depicted in Figs. 11 and 12. The optical band gap decreases as the percentage of GO increases. The results indicate that the introduction of a small amount of GO doping into the PVA structure lowers the activation energy within the polymer chain, thereby enhancing ionic conductivity. Pure PVA exhibits an optical band gap of 2.2 eV, while the optical characteristics of PVA/GO reveal that the band gap energy for the 0.3 wt.%

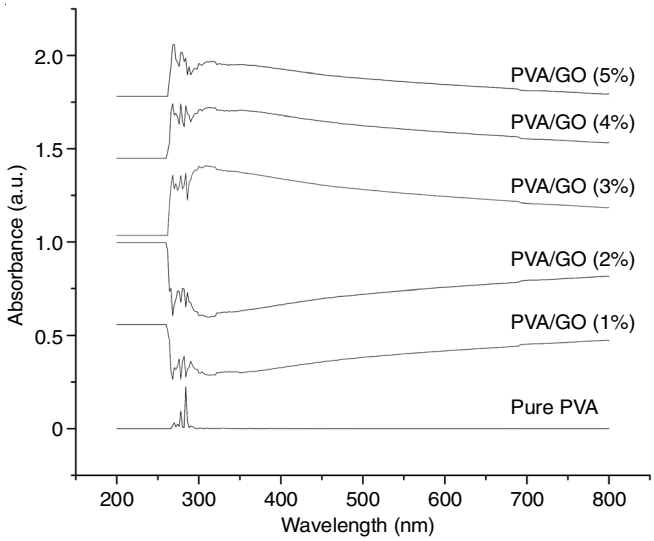

Fig. 9. UV-Vis analysis spectra of PVA and PVA/GO nanocomposites

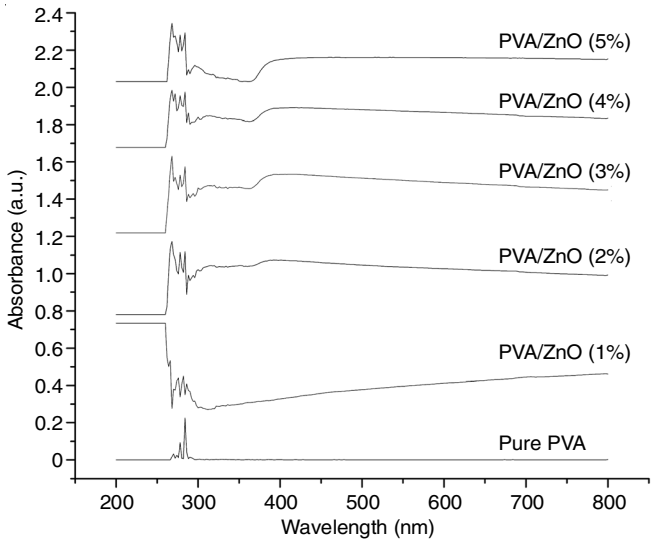

Fig. 10. UV-Vis analysis spectra of PVA/ZnO

composition is the lowest at 1.99 eV among all tested ratios. Consequently, as the weight percentage of GO increases, both the band edge and direct band gap values decrease, suggesting that GO contributes to the defects present in the polymer films.

Fig. 10 illustrates the absorbance profile of PVA/ZnO nanocomposite films. The incorporation of nano ZnO into the PVA matrix results in a reduction of transmittance in the UV-visible range, as depicted in Fig. 10. Within the 200-800 nm range, the PVA solution shows no visible absorption, whereas the PVA/ZnO nanoparticle solutions exhibit an absorption peak around 280 nm. The results indicate that the addition of ZnO does not significantly affect its absorption characteristics. The excitonic peaks in the absorption spectra are not prominently visible due to the limited quantity of integrated nanoparticles. From Figs. 13 and 14, it is observed that the concentration of ZnO nanoparticles increases, the absorption edge shifts systematically towards longer wavelengths or lower energies, corresponding to the blue-green region of the visible spectrum. The notable change in energy observed can be attributed to the development

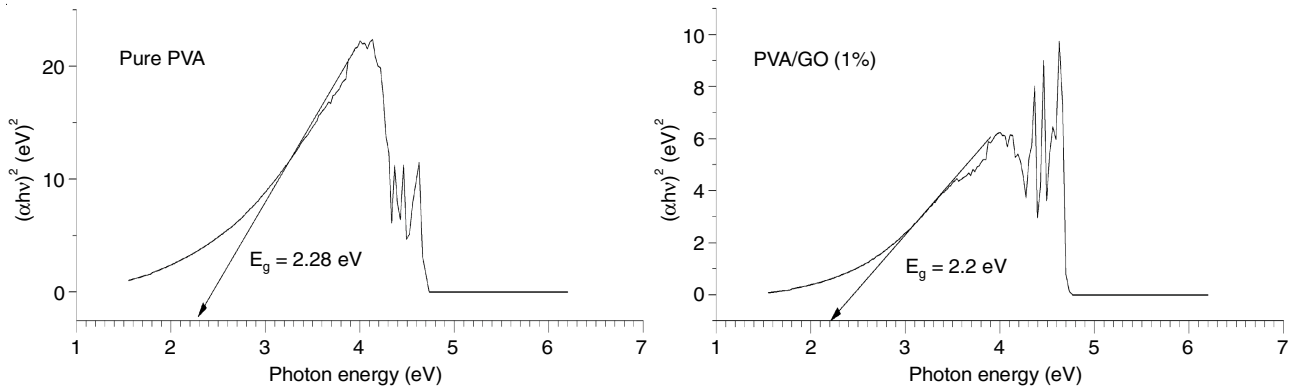

Fig. 11. Tauc plot for PVA and PVA/GO (1%) nanocomposites

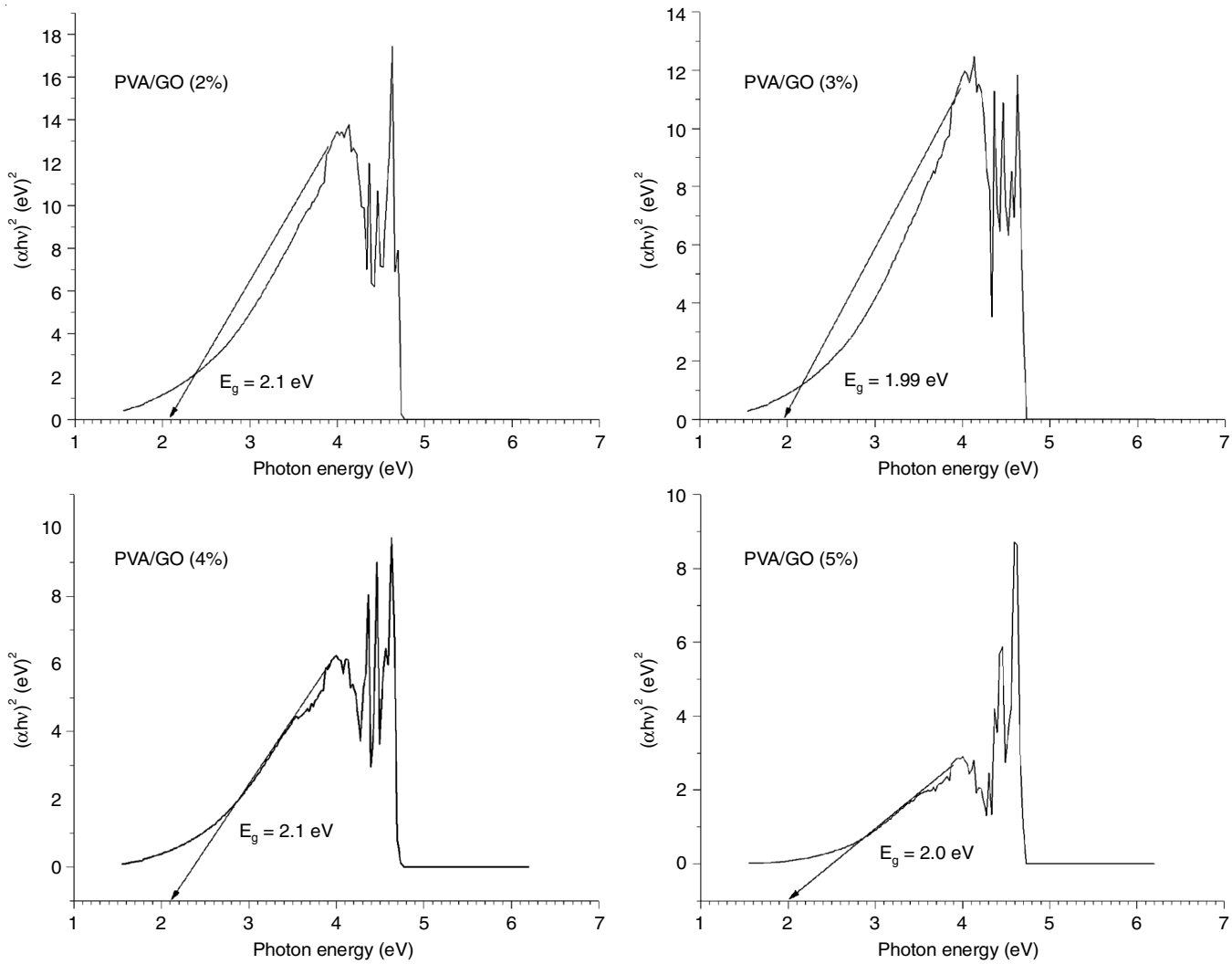

Fig. 12. Tauc plot for PVA/GO (2%, 3%, 4% and 5%) nanocomposites

of micro-strain within the PVA/ZnO composite matrix, which alters the energy band structure of the ZnO nanoparticles, as reflected in the edge transition. Another possible explanation for this change is the emergence of additional defect states in the energy gap resulting from variations in the weight percentage of nano ZnO [43-45].

Direct band gap values were estimated from the plots of ($\alpha h\nu^2$) against hν, with the corresponding band gap values. This analysis aims to elucidate the impact of indirect transitions in nanocomposite films resulting from the incorporation of filler nano ZnO into the polymer matrix. The observed reduction in band gap may stem from two distinct mechanisms. The first mechanism involves the formation of donor levels at the lower end of the conduction band, which is attributed to the tensile strain experienced by the composite films [46]. The second mechanism relates to the introduction of defects within the

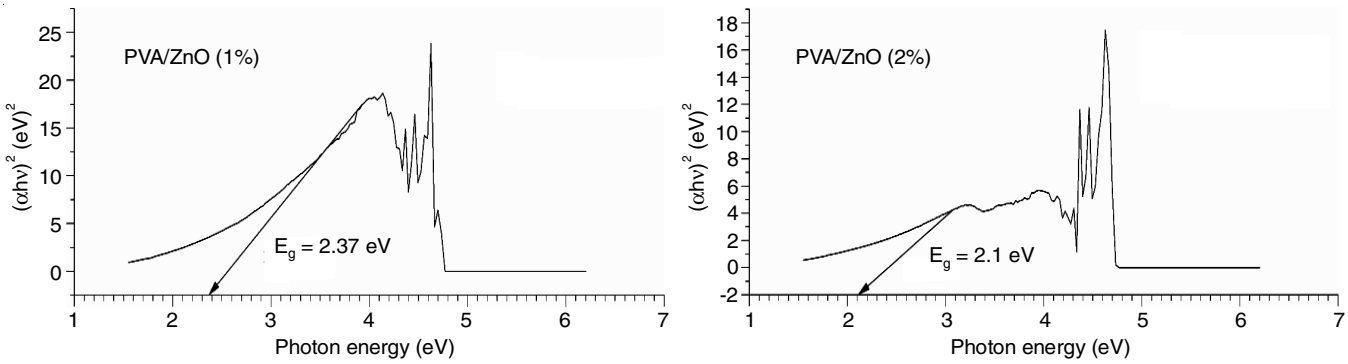

Fig. 13. Tauc plot for PVA/ZnO (1% & 2%) nanocomposites

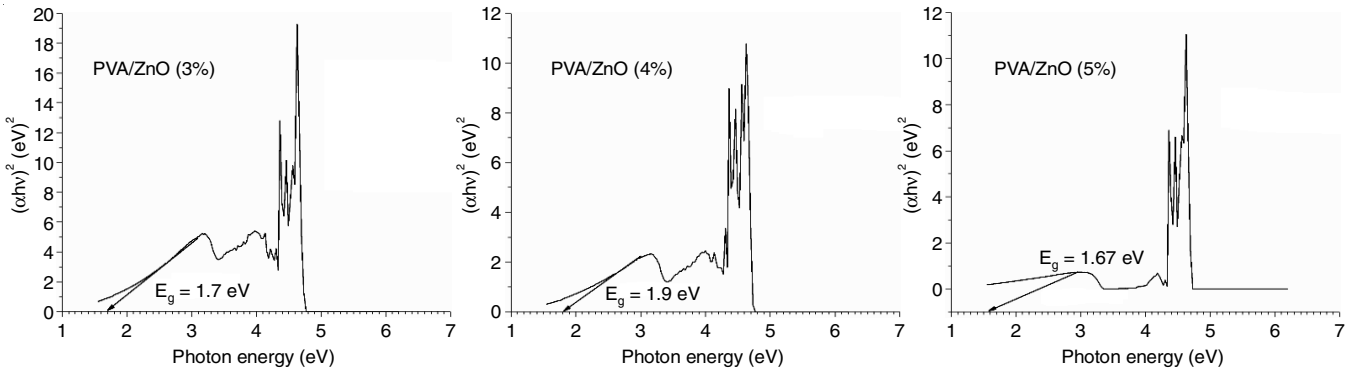

Fig. 14. Tauc plot for PVA/ZnO (3%, 4% & 5%) nanocomposites

polymer matrix. As the doping level (filler concentration) in the polymer matrix increases, these defects create localized states within the optical band gap (Table-4), leading to a reduction in the energy band gap [41,47]. Since direct band gap transitions are facilitated by the photon interactions, the size of the optical energy gap diminishes in allowed direct band gap transitions [48]. The overall effect of varying filler concentration on the optical band gap energy is associated with the structural morphologies, particle size and surface microstructure of the nano fillers, which have modified the composition of the host PVA polymer. An increase in both GO and ZnO concentrations leads to a rise in the absorption coefficient and a decrease in the optical band gap of the nanocomposite films, indicating their potential applicability in optoelectronic devices.

TABLE-4
ENERGY BAND GAP OF PVA, PVA/GO AND PVA/ZnO NANOCOMPOSITES

Sample name	Band gap (eV)	Sample name	Band gap (eV)
Pure PVA	2.20	PVA/ZnO (1%)	2.37
PVA/GO (1%)	2.28	PVA/ZnO (2%)	2.10
PVA/GO (2%)	2.10	PVA/ZnO (3%)	1.70
PVA/GO (3%)	1.99	PVA/ZnO (4%)	1.90
PVA/GO (4%)	2.10	PVA/ZnO (5%)	1.67
PVA/GO (5%)	2.00		

Electrical properties: The direct current (DC) conductivity of PVA, PVA/GO and PVA/ZnO nanocomposites was examined at room temperature utilizing the four-probe technique. Figs. 15 and 16 illustrate the relationship between electrical conductivity and the weight percentage of ZnO nanoparticles. A noticeable increase in the conductivity of PVA was observed following the incorporation of GO and ZnO nanoparticles, in comparison to pure PVA. It was determined that the added nanoparticles facilitated the formation of conductive pathways through newly established charge transfer complexes within the PVA matrix, resulting in enhanced conductivity [49]. Upon reviewing Table-5, it was concluded that the inclusion of GO and ZnO nanoparticles contributed to the development of conductive pathways within the PVA matrix, leading to an increase in conductivity.

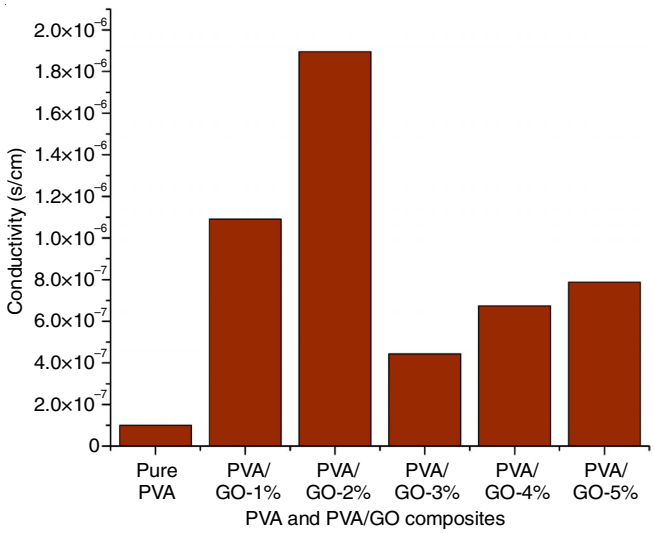

Fig. 15. Electrical conductivity of PVA and PVA/GO nanocomposites

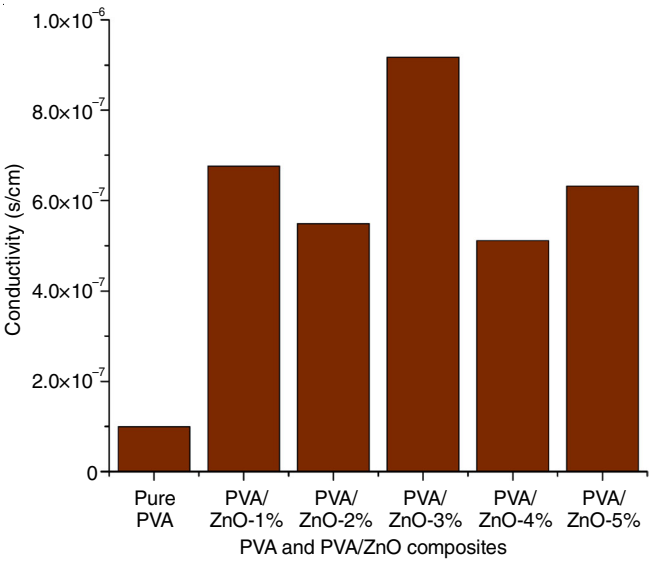

Fig. 16. Electrical conductivity of PVA and PVA/GO nanocomposites

TABLE-5
ELECTRICAL CONDUCTIVITY OF PVA, PVA/GO AND PVA/ZnO NANOCOMPOSITES

Sample name	Conductivity (s cm^{-1})	Sample name	Conductivity (s cm^{-1})
Pure PVA	9.952×10^{-8}	PVA/ZnO (1%)	6.760×10^{-6}
PVA/GO (1%)	1.0906×10^{-6}	PVA/ZnO (2%)	5.490×10^{-7}
PVA/GO (2%)	1.895×10^{-6}	PVA/ZnO (3%)	9.168×10^{-7}
PVA/GO (3%)	4.423×10^{-7}	PVA/ZnO (4%)	5.111×10^{-7}
PVA/GO (4%)	6.747×10^{-7}	PVA/ZnO (5%)	6.318×10^{-7}
PVA/GO (5%)	7.882×10^{-7}		

Conclusion

The solution casting method was effectively employed to prepare various samples of PVA/GO and PVA/ZnO polymer nanocomposites, incorporating different weight percentages of nanoparticles ranging from 1% to 5%. Each sample was characterized with XRD, FTIR, UV-Vis, thermomechanical analysis and electrical measurements, with the results thoroughly examined. The incorporation of GO and ZnO nanoparticles into the PVA nanocomposite films was clearly evidenced and validated through XRD and FTIR analyses. The mechanical properties of the PVA nanocomposites containing nanoparticles exhibited superior performance compared to pure PVA. Specifically, the tensile strength increased from 3.859 MPa to 9.613 MPa with the addition of GO and to 9.307 MPa with ZnO. Significantly, GO demonstrated slightly enhanced mechanical properties compared to ZnO within the PVA matrix. The thermal stability of the composites improved with the inclusion of both nanoparticles. Pure PVA experienced a weight loss of 94.10% at 600 ºC, which decreased to 88.93% for PVA/GO and 86.36% for PVA/ZnO, indicating a significant enhancement in thermal properties due to the incorporation of these nanoparticles. The optical band gap was observed to decrease with the addition of nanoparticles in the PVA matrix, as confirmed by UV analysis. Similarly, the electrical conductivity increased to 1.895×10^{-6} S/cm with GO and 6.38×10^{-6} S/cm with ZnO, compared to a conductivity value of 9.952×10^{-7} S/cm for pure PVA.

CONFLICT OF INTEREST

The authors declare that there is no conflict of interests regarding the publication of this article.

REFERENCES

1. K.A. Williams, A.J. Boydstona and C.W. Bielawski, *Chem. Soc. Rev.*, **36**, 729 (2007); https://doi.org/10.1039/B601574N
2. J.D. Fowler, M.J. Allen, V.C. Tung, Y. Yang, R.B. Kaner and B.H. Weiller, *ACS Nano*, **3**, 301 (2009); https://doi.org/10.1021/nn800593m
3. M. Liang, M. Zhi and L. Zhi, *J. Mater. Chem.*, **19**, 5871 (2009); https://doi.org/10.1039/b901551e
4. S. Gahlot, P.P. Sharma, V. Kulshrestha and P.K. Jha, *ACS Appl. Mater. Interfaces*, **6**, 5595 (2014); https://doi.org/10.1021/am5000504
5. S. Gahlot and V. Kulshrestha, *ACS Appl. Mater. Interfaces*, **7**, 264 (2015); https://doi.org/10.1021/am506033c
6. S. Gahlot, P.P. Sharma and V. Kulshrestha, *Sep. Sci. Technol.*, **50**, 446 (2015); https://doi.org/10.1080/01496395.2014.973525
7. K.S. Hemalatha, N. Parvatikar and K. Rukmani, *Int. J. Adv. Sci. Tech.*, **5**, 106 (2014); https://doi.org/10.3923/jeasci.2019.717.724
8. J. Liang, Y. Huang, L. Zhang, Y. Wang, Y. Ma, T. Guo and Y. Chen, *Adv. Funct. Mater.*, **19**, 2297 (2009); https://doi.org/10.1002/adfm.200801776
9. L. Zhang, Z. Wang, C. Xu, Y. Li, J. Gao, W. Wang and Y. Liu, *J. Mater. Chem.*, **21**, 10399 (2011); https://doi.org/10.1039/c0jm04043f
10. K.M. Abu Hurayra–Lizu, M.W. Bari, F. Gulshan and M.R. Islam, *Heliyon*, **7**, e06983 (2021); https://doi.org/10.1016/j.heliyon.2021.e06983
11. H.J. Salavagione, G. Martínez and M.A. Gómez, *J. Mater. Chem.*, **19**, 5027 (2009); https://doi.org/10.1039/b904232f
12. H.M. Kim, J.K. Lee and H.S. Lee, *Thin Solid Films*, **519**, 7766 (2011); https://doi.org/10.1016/j.tsf.2011.06.016
13. N. Wang, P.R. Chang, P. Zheng and X. Ma, *Appl. Surf. Sci.*, **314**, 815 (2014); https://doi.org/10.1016/j.apsusc.2014.07.075
14. X. Zhao, Q. Zhang, D. Chen and P. Lu, *Macromolecules*, **43**, 2357 (2010); https://doi.org/10.1021/ma902862u
15. S. Safa, R. Sarraf-Mamoori and R. Azimirad, *Adv. Mater. Res.*, **829**, 577 (2013); https://doi.org/10.4028/www.scientific.net/AMR.829.577
16. S. Raha and M. Ahmaruzzaman, *Nanoscale Adv.*, **4**, 1868 (2022); https://doi.org/10.1039/D1NA00880C
17. Z.L. Wang, *Mater. Today*, **7**, 26 (2004); https://doi.org/10.1016/S1369-7021(04)00286-X
18. A. Sedghi and N. Riyahi Noori, *J. Ceram. Process. Res.*, **12**, 752 (2011).
19. S.A. Kumar and S.-M. Chen, *Anal. Lett.*, **41**, 141 (2008); https://doi.org/10.1080/00032710701792612
20. R.G. Singh, N. Gautam, S.K. Gautam, V. Kumar, A. Kapoor and F. Singh, *J. Renew. Sustain. Energy*, **5**, 033134 (2013); https://doi.org/10.1063/1.4811818
21. S. Padinhattayil and K.S. Rai, *Asian J. Chem.*, **32**, 881 (2020); https://doi.org/10.14233/ajchem.2020.22483
22. W.S. Hummers Jr. and R.E. Offeman, *J. Am. Chem. Soc.*, **80**, 1339 (1958); https://doi.org/10.1021/ja01539a017
23. W.M. Itano, J.J. Bollinger, J.N. Tan, B. Jelenkovic, X.-P. Huang and D.J. Wineland, *Science*, **279**, 686 (1998); https://doi.org/10.1126/science.279.5351.686
24. S.G. Rathod, R.F. Bhajantri, V. Ravindrachary, P.K. Pujari and T. Sheela, *J. Adv. Dielectr.*, **4**, 1450033 (2014); https://doi.org/10.1142/S2010135X14500337

25. S.H. Rashmi, A. Raizada, G.M. Madhu, A.A. Kittur, R. Suresh and H.K. Sudhina, *Plast. Rubber Compos.*, **44**, 33 (2015); https://doi.org/10.1179/1743289814Y.0000000115
26. J. Li, L. Shao, L. Yuan and Y. Wang, *Mater. Des.*, **54**, 520 (2014); https://doi.org/10.1016/j.matdes.2013.08.090
27. J. Wang, C. Gao, Y. Zhang and Y. Wan, *Mater. Sci. Eng. C*, **30**, 214 (2010); https://doi.org/10.1016/j.msec.2009.10.006
28. C.C. Yang, Y.J. Lee and J.M. Yang, *J. Power Sources*, **188**, 30 (2009); https://doi.org/10.1016/j.jpowsour.2008.11.098
29. J. George, K.V. Ramana, A.S. Bawa and Siddaramaiah, *Int. J. Biol. Macromol.*, **48**, 50 (2011); https://doi.org/10.1016/j.ijbiomac.2010.09.013
30. X.M. Sui, C.L. Shao and Y.C. Liu, *Appl. Phys. Lett.*, **87**, 113115 (2005); https://doi.org/10.1063/1.2048808
31. H.N. Chandrakala, B. Ramaraj, S. Shivakumaraiah, G.M. Madhu and F.N.M. Siddaramaiah, *J. Mater. Sci.*, **47**, 8076 (2012); https://doi.org/10.1007/s10853-012-6701-y
32. S.C. Liufu, H.N. Xiao and Y.P. Li, *Polym. Degrad. Stab.*, **87**, 103 (2005); https://doi.org/10.1016/j.polymdegradstab.2004.07.011
33. T.E. Motaung, A.S. Luyt, F. Bondioli, M. Messori, M.L. Saladino, A. Spinella, G. Nasillo and E. Caponetti, *Polym. Degrad. Stab.*, **97**, 1325 (2012); https://doi.org/10.1016/j.polymdegradstab.2012.05.022
34. T. Ramanathan, A.A. Abdala, S. Stankovich, D.A. Dikin, M. Herrera-Alonso, R.D. Piner, D.H. Adamson, H.C. Schniepp, X. Chen, R.S. Ruoff, S.T. Nguyen, I.A. Aksay, R.K. Prud'Homme and L.C. Brinson, *Nat. Nanotechnol.*, **3**, 327 (2008); https://doi.org/10.1038/nnano.2008.96
35. S.S. Ray and M. Bousmina, *Macromol. Chem. Phys.*, **207**, 1207 (2006); https://doi.org/10.1002/macp.200600163
36. C. Lee, X. Wei, J.W. Kysar and J. Hone, *Science*, **321**, 385 (2008); https://doi.org/10.1126/science.1157996
37. C. Gómez-Navarro, M. Burghard and K. Kern, *Nano Lett.*, **8**, 2045 (2008); https://doi.org/10.1021/nl801384y
38. X. Li, Y. Xing, Y. Jiang, Y. Ding and W. Li, *Int. J. Food Sci. Technol.*, **44**, 2161 (2009); https://doi.org/10.1111/j.1365-2621.2009.02055.x
39. P.W. Davis and T.S. Shilliday, *Phys. Rev.*, **118**, 1020 (1960); https://doi.org/10.1103/PhysRev.118.1020
40. A.B. Bourlinos, D. Gournis, D. Petridis, T. Szabó, A. Szeri and I. Dékány, *Langmuir*, **19**, 6050 (2003); https://doi.org/10.1021/la026525h
41. N. Rajeswari, S. Selvasekarapandian, C. Sanjeeviraja, J. Kawamura and S. Asath Bahadur, *Polym. Bull.*, **71**, 1061 (2014); https://doi.org/10.1007/s00289-014-1111-8
42. G.K.M. Thutupalli and S.G. Tomlin, *J. Phys. D Appl. Phys.*, **9**, 1639 (1976); https://doi.org/10.1088/0022-3727/9/11/010
43. S.S. Nair, M. Mathews and M.R. Anantharaman, *Chem. Phys. Lett.*, **406**, 398 (2005); https://doi.org/10.1016/j.cplett.2005.02.107
44. B. Suo, X. Su, J. Wu, D. Chen, A. Wang and Z. Guo, *Mater. Chem. Phys.*, **119**, 237 (2010); https://doi.org/10.1016/j.matchemphys.2009.08.054
45. S. Dutta and B.N. Ganguly, *J. Nanobiotechnol.*, **10**, 29 (2012); https://doi.org/10.1186/1477-3155-10-29
46. J. Kayathri, N. RaniMeiyammai, S. Rani, K.P. Bhuvana, K. Palanivelu and S.K. Nayak, *J. Mater.*, **2013**, 473217 (2013); https://doi.org/10.1155/2013/473217
47. B.D. Cullity and R.J.P.T. Smoluchowski, *Phys. Today*, **10**, 50 (1957); https://doi.org/10.1063/1.3060306
48. R. Vijaya Kumar, R. Elgamiel, Y. Diamant, A. Gedanken and J. Norwig, *Langmuir*, **17**, 1406 (2001); https://doi.org/10.1021/la001331s
49. S. Mahendia, A.K. Tomar and S. Kumar, *J. Alloys Compd.*, **508**, 406 (2010); https://doi.org/10.1016/j.jallcom.2010.08.075